Research Paper

Application of the Ultrasonic Ring Array Used in UTT for the Reflection Method Examinations of Structures

Wiktor STASZEWSKI[(1), (2)*], Tadeusz GUDRA[(1)], Krzysztof J. OPIELIŃSKI[(1)]

[(1)] *Department of Acoustics and Multimedia, Faculty of Electronics, Wrocław University of Science and Technology*
Wrocław, Poland; e-mail: {tadeusz.gudra, krzysztof.opielinski}@pwr.edu.pl
*Corresponding Author e-mail: wiktor.staszewski@pwr.edu.pl

[(2)] *T. Marciniak Lower Silesian Specjalist Hospital – Emergency Medicine Centre*
Wrocław, Poland

The ultrasonic ring array, designed for examining the female breast with the use of ultrasonic transmission tomography (UTT), has been adapted for reflection method trials. By altering the activation time of ultrasonic elementary transducers, the parameters of the focus were changed with the aim at improving the quality of the obtained ultrasound image. For this purpose, a phantom consisting of rods having varying thicknesses was analyzed when moving the position of the focus with the use of dynamic focusing along the symmetry axis of the ring array ranging from 30 to 130 mm from central transducers. In previous trials, which applied an algorithm using the sum of all the acoustic fields, a series of simulations was performed in conditions identical to the phantom trial. This paper documents attempts at improving the parameters of the acoustic field distribution during unconventional focusing. The research here presented is a continuation of examinations focusing on the acoustic field distribution inside the ultrasonic ring array with the aim at finding the best possible cross-section of the female breast using the reflection method.

Keywords: ultrasonic reflection tomography; dynamic focusing; ultrasonic ring array.

1. Introduction

The incidence rates of breast cancer continued to increase between 1980 and 2015. The development of effective diagnostic methods contributes to the detection of lesions at their early development stages. Several research centers around the world are currently working on prototypes of ultrasound tomography scanners which would allow noninvasive and safe imaging of the structure of the female breast (BIRK *et al.*, 2016; DURIC *et al.*, 2007a; 2013; GUDRA, Opieliński, 2006a; 2006b; 2006c; JIRIK *et al.*, 2012; MARMARELIS *et al.*, 2007; OPIELIŃSKI *et al.*, 2015; 2016; WISKIN *et al.*, 2013). Breast diagnostics with the new ultrasound tomography scanner is painless, noninvasive and completely safe, and therefore it can be performed repeatedly, with no risk for the patient. An ultrasonic ring array has been developed at Wroclaw University of Science and Technology in order to perform *in vivo* examinations of female breasts (GUDRA, Opieliński, 2006a; 2006b; 2006c; 2016, OPIELIŃSKI *et al.*, 2014; 2015; 2016; 2018). A private Polish company used the patented solution (GUDRA, OPIELIŃSKI, 2009) to construct the first prototype of an ultrasonic transmission tomography scanner for female breast examinations. This research focuses on an attempt at ultrasound imaging with the use of a ring array adapted to ultrasonic transmission tomography performed at the operating frequency of individual transducers equal to 2 MHz. From the practical point of view, the operating frequency of the elementary ultrasound transducers equal to 2 MHz proves to be too low during a classical ultrasound imaging, which is performed at frequencies equal to 5–6 MHz. The echographic method is commonly used in medicine to characterize and visualize biological media. In the case of an ultrasonic ring array, this method is based on the fact that each of the elementary ultrasound transmitter-receiver transducers generates a transmission pulse into the biological medium, which is then reflected at the border

of structures having different acoustic impedances and returned to the transducer. Identifying the locations of the borders of those structures in the medium is possible owing to the different echo return times. The image is displayed as shades of gray and the amplitude of the echoes is proportional to the reflection coefficient value.

The ultrasound tomography scanner scans the entire breast using ultrasound waves coming from many directions around it and on many levels. Subsequently, it processes the obtained data and reconstructs images of individual coronal breast sections in layers of several millimeters. Their omnidirectional fusing with the use of the compound imaging (CI) (ENTREKIN *et al.*, 1999; OPIELIŃSKI *et al.*, 2014) method with overlaying allows the elimination of noise and image distortions as a result of averaging common pixel areas. This article is a continuation of prior research (STASZEWSKI *et al.*, 2018; 2019; STASZEWSKI, GUDRA, 2019), which investigated an optimum number of transducers, and the beam focusing and deflection method, which would result in the possibly best image of a female breast cross-section. In previously published works, the authors presented an extensive analysis of the acoustic field distribution inside the analyzed array. This paper presents the results of measurements performed on a phantom during dynamic focusing and successively using 32 sections (each containing 32 transducers) of the ultrasonic ring array. It also describes an attempt at improving the acoustic parameters of the focused ultrasound beam generated by individual sections.

2. Construction of the ultrasonic ring array

An ultrasonic ring array comprises 1024 elementary ultrasonic transducers working at a frequency of approx. 2 MHz (GUDRA, OPIELIŃSKI, 2006a; 2006b; 2006c; OPIELIŃSKI *et al.*, 2015; 2018). The transducers are rectangular plates 0.5×18 mm in size and about 1 mm in thickness. They are arranged at equal distances of 0.3 mm with pitch of 0.8 mm, on the inner side of the ring which has a radius R_p = 130 mm. Each of the elementary transducers can function as both a transmitter and a receiver. Figure 1 shows
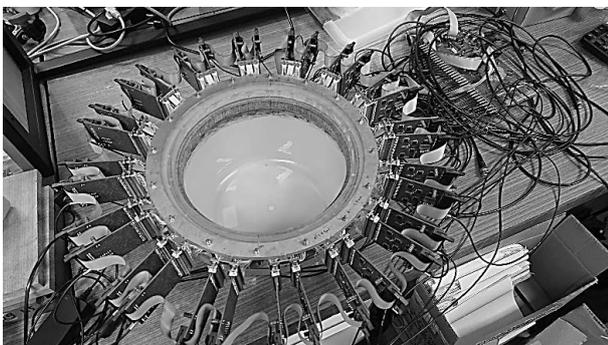
Fig. 1. A top view of one of the first prototypes of the ultrasonic ring array.

a prototype of one of the ultrasonic ring arrays constructed on the basis of the patented solution (GUDRA, OPIELIŃSKI, 2009).

3. Calculation method

The acoustic field distribution generated by the curvilinear array of elementary ultrasonic transducers located on the inner side of the ring was calculated by summing the complex values of the acoustic fields generated by each transducer in the sector.

The model is based on an assumption that all ultrasonic transducers are identical and have the same efficiency (OPIELIŃSKI, 2011). For example, the pressure value in point 5 is calculated by summing the complex values of pressure in points 1–9 for one transducer (Fig. 2).
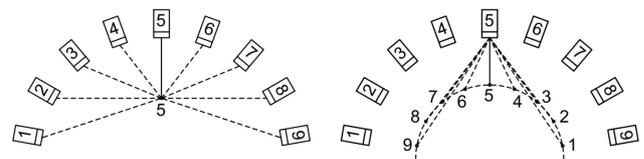
Fig. 2. Method for calculating the acoustic field distribution by summing the fields for a section consisting of 9 ultrasonic transducers.

For a sector of a multi-element ring array, an original algorithm was used for numerically determining the pressure distribution of the ultrasonic wave at points P (R, θ, φ) of any plane of the medium in the far field, generated by a curvilinear array of rectangular ultrasonic transducers. The wave pressure distribution was calculated as a complex sum of geometric transformations of the fields calculated for all elementary transducers in the sector (Fig. 2). This aim was achieved by using an algorithm demonstrated in (OPIELIŃSKI, 2011):

$$p = \left| \sum_{i=0}^{n-1} -\frac{j\rho c k V_a}{2\pi R_i} abe^{j(\omega t - kR_i)} \left[\frac{\sin\left(\frac{u_i a}{2}\right)}{\frac{u_i a}{2}} \right] \left[\frac{\sin\left(\frac{wb}{2}\right)}{\frac{wb}{2}} \right] \right|, \quad (1)$$

where ρ – medium density, c – propagation speed of an ultrasonic wave in the medium, $k = 2\pi/\lambda$ – wave number, $\lambda = c/f$ – wavelength, f – ultrasonic frequency, $\omega = 2\pi f$ – angular vibration frequency, t – time, V_a – acoustic speed, a – width of the elementary rectangular ultrasonic transducer, b – height of the elementary rectangular ultrasonic transducer, $u_i = 2\pi \cdot \sin(\theta_i)/\lambda$, $w = 2\pi \cdot \sin(\varphi)/\lambda$, R_i, θ_i, φ – polar coordinates of point P (R, θ, φ), adequately corrected with respect to the position of the $(i+1)$-th transducer in the sector (see (OPIELIŃSKI, 2011; STASZEWSKI *et al.*, 2019)).

For the resonance frequency f_r = 2 MHz, the near-field range in the horizontal plane of a rectangular elementary transducer having width a = 0.5 mm is $l_o = 0.35a^2/\lambda \approx 0.12$ mm.

The analysis of the acoustic field distribution for the linear echographic scanning method in individual sections of a ring array having a different number of activated ultrasonic transducers is based on calculations of the value of the acoustic pressure level, assuming the reference pressure value used in hydroacoustics $p_o = 1\ \mu$Pa. The sound pressure level was calculated according to the following equation:

$$L_p = 20 \log\left(\frac{p(x,0,z)}{p_o}\right). \qquad (2)$$

The acoustic pressure $p(x,0,z)$ in the horizontal plane, in the mid-height of the transducers (for angle $\varphi = 0$) was calculated from Eqs (1) and (2). Attenuation in water was not included in the calculations due to its negligible effect on the results. The calculations were performed in the range x from –130 mm to 130 mm and from 0 mm to 260 mm. Due to the assumed even number n of the transducers in the section and in order to maintain symmetry, the *XYZ* coordinate system was rotated in the horizontal plane by an angle allowing the center of the system to be positioned in the symmetry axis of the transducer section. The set range of the x and z values allows the visualization of the acoustic field distribution in the entire area of the inside of the ring array having radius $R_p = 130$ mm. The complex three-dimensional matrices containing complex values of the acoustic pressure level were summed using MATLAB software, which is an excellent software environment for performing this type of calculations (PRATAP, 2013).

The visual qualitative assessment step is necessary in order to identify those important features of the imaging system which may prove difficult to detect with the use of a limited set of quantitative parameters. The visual assessment was performed for a number of output images (COSTARIDOU, 2005; KAK, SLANEY, 2001):

a) presence of artifacts not related to the set impedance ratio,

b) presence of heterogenous artifacts (e.g. intrusions),

c) the scale of random disturbances (variance, granularity, arrangement),

d) inclusion imaging contrast,

e) slope inclination on the border of the inclusion.

Visual evaluation of the results on the basis of the images is difficult and therefore quantitative parameters were analyzed (KAK, SLANEY, 2001):

• average value – the average grayscale level from pixels $I_1,...,I_N$ on an ultrasound image

$$\overline{I} = \frac{1}{n} \sum_{j=1}^{N} I_j, \qquad (3)$$

• standard deviation

$$\sigma = \sqrt{\frac{1}{N-1} \sum_{j+1}^{N} (I_j - \overline{I})^2}, \qquad (4)$$

• contrast

$$f_k = \sum_{i=1}^{N_g-1} n^2 \left\{ \sum_{\substack{i=1 \\ |i=j|=n}}^{N_g} \sum_{j=1}^{N_g} p(i,j) \right\}, \qquad (5)$$

where n is a number of pixel in the image, N_g is number of gray levels in the image.

4. Results

During the measurements, which were performed with the use of an ultrasonic ring array, all sectors of the ultrasonic array were successively excited using the full capabilities of the array, i.e. $n = 1024$ ultrasonic transducers were excited. The images were fused with the *Compound Imaging* (CI) method. They were fused omnidirectionally with overlaying 32 images when successively exciting 32 sections consisting of $n = 32$ transducers (OPIELIŃSKI *et al.*, 2014). During the measurements, the array was immersed in distilled water having a temperature of 25°C. The tests were performed while moving the focus from 30 mm to 130 mm at 20 mm steps along the diameter of the ring array. During the tests, the phantom was placed in the center of the array, in the focal point resulting from the natural curvature of the transducer matrix. The phantom consisted of 6 rods. Figure 3 shows a schematic top view of the phantom.
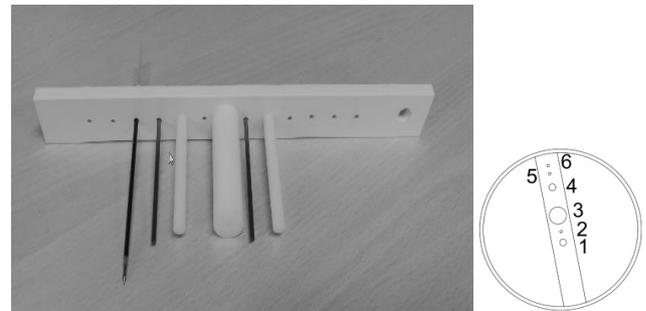
Fig. 3. Top view of the phantom which served for the measurements and a schematic top view of the location of the phantom with respect to the ultrasonic ring array together with rod numbers.

Rods 1, 3, and 4 were made of ertacetal, rods 2 and 5 were made of brass, and rod 6 was a pen refill. The diameters of the rods were as follows: rod 1–10 mm, rod 2–2 mm, rod 3–25 mm, rod 4–10 mm, rod 5–2 mm and rod 6–2 mm. Spacing of holes in the stand measured 17 mm (from left to right): rod 1–3 mm, rod 2–3 mm, rod 3–8.25 mm, rod 4–20 mm, rod 5–3 mm, rod 6–8.25 mm.

Figure 4 shows the results of the measurements performed with the ultrasonic ring array. The brightness of the images was increased by 30%.
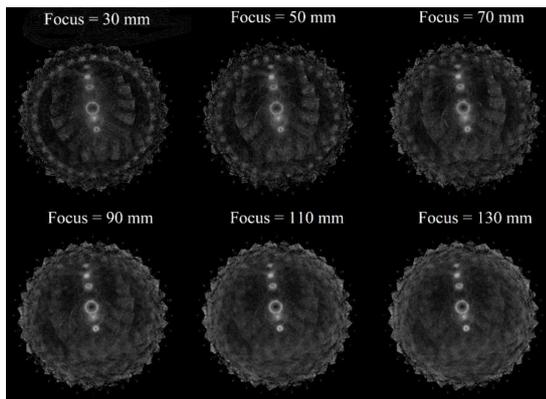
Fig. 4. The results of phantom measurements performed with the use of the ultrasonic ring array and based on the Compound Imaging method for the focal point at distances $R = 30, 50, 70, 90, 110$, and 130 mm.

An analysis of the ultrasound images presented in Fig. 4 reveals numerous areas in the image where noise occurs directly at the ultrasonic transducers. The 32 sections were assembled in the form of ultrasound images by arithmetically averaging the values of overlapping pixels. Each individual ultrasound image was visualized in gray scale values after logarithm, as in a standard ultrasound machine. As the distance between the focal point and the central transducers increases, the amount of noise can be observed to increase and the distortion regions – to become more distinct. Figure 5 shows a 3D visualization of an ultrasound image for $R = 130$ mm, with the grayscale in the z axis being from 0 to 255.
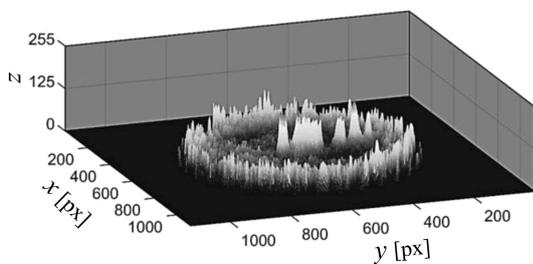
Fig. 5. 3D visualization of the phantom measurements for dynamic focusing at a distance $R = 130$ mm.

Figure 5 shows distinct echoes from the rods of the phantom. The maxima from the ultrasonic transducers around the circumference of the ring matrix of the ultrasonic array are also visible. For a more detailed analysis, the investigations focused solely on the fragment of the ultrasound image containing only echoes from the phantom rods. Thus, the graphical analysis of the image refers to the average background value recorded around the analyzed inclusions. Figure 6 shows a graphical analysis of the echoes from the
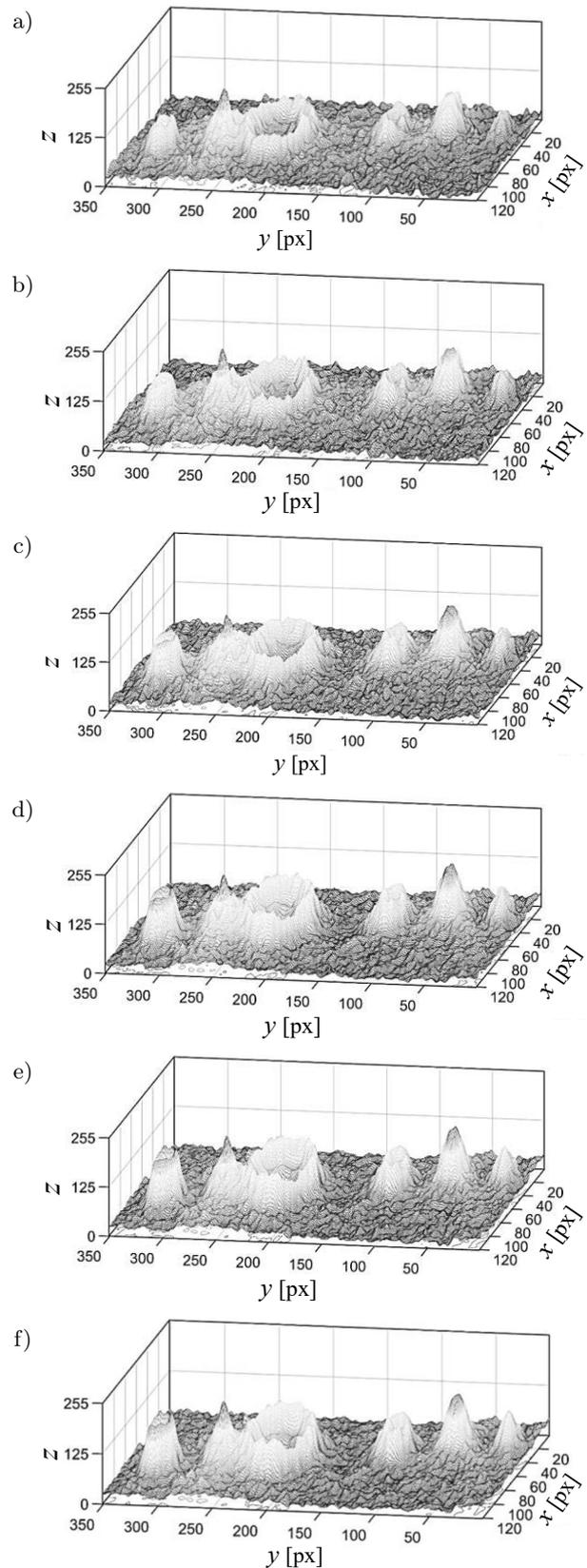
Fig. 6. 3D visualization of the measurements performed for a phantom positioned centrally in the focal point, for a fragment of the image comprising echoes from the rods, and for dynamic focusing settings at distances $R = 30, 50, 70, 90, 110$, and 130 mm.

rods of the phantom. As in the previous graph, the third parameter in the z axis is the grayscale. The graphs served to generate the cross-section of the tested inclusions, to identify the ratio of the inclusion brightness to the background level, and to calculate three measures of the image qualitative evaluation in grayscale with respect to individual pixels: average value, standard deviation and contrast. The cross-sections (Fig. 7) were generated along the y axis, on which the pixel numbering is marked in accordance with the analyzed ultrasound image (Fig. 5), while the vertical axis represents the brightness maximum as per
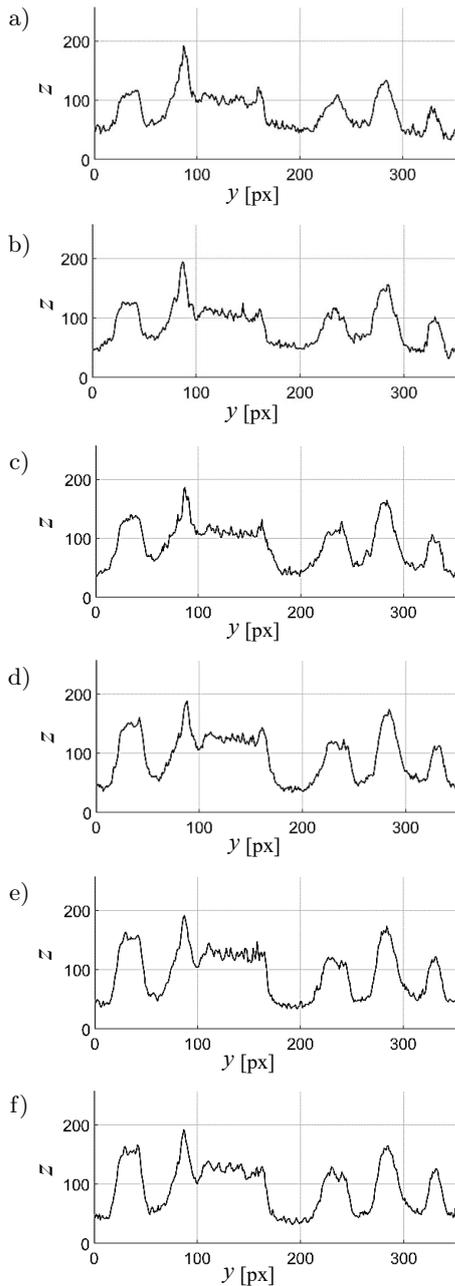
the grayscale and corresponding to the particular row of pixels in accordance with the numbers in axis y.

Based on the graphs showing the echo amplitudes from individual phantom rods (Figs 6 and 7) and on the ratio of the echo brightness to the noise level (Table 1), the ratio of the background to the echo was found to decrease as the focusing distance from the central transducers increases. The best results were recorded for the focusing at a distance of 110 and 130 mm from the central transducers. The highest background to echo ratio was observed in the case of rod 1–25.93% for the focusing 130 mm from the central transducers. A more favourable ratio of noise level to the brightness of the echo from the intrusion should mean that these images will have a better contrast. In order to confirm this expected effect, the quantitative parameters of the image were calculated (Table 2).

Table 1. The ratio of the average noise level to the brightness of the inclusion from the phantom rod, represented as percentage ($\Delta = 0.01$).

Radius R [mm]	Rod number						Average value
	1	2	3	4	5	6	
30	48.25	33.85	47.32	48.62	38.64	48.84	44.59
50	46.88	36.13	48.18	43.10	37.74	44.12	42.69
70	34.59	34.95	38.39	43.55	32.93	50.94	39.22
90	29.03	32.98	33.08	34.78	36.47	47.79	35.69
110	27.04	29.32	31.25	33.61	34.75	41.32	32.88
130	25.93	28.65	32.81	29.92	32.93	39.20	31.57

Table 2. Parameters for the quantitative assessment of ultrasound images.

R [mm]	30	50	70	90	110	130
$\bar{I}$	0.3678	0.3908	0.4033	0.4250	0.4246	0.4260
σ	0.1336	0.1502	0.1580	0.1705	0.1721	0.1728
f_k	0.5843	0.5979	0.5647	0.5569	0.5765	0.5882

The average brightness value of the pixels in the image and the value of the standard deviation increase together with the increase in the focusing distance from the central transducers, and as a result the differences between the recorded ultrasound images also increase. The best contrast was found in the image when the focusing was 50 mm from the central transducers. This result does not confirm the fact that a decrease in the ratio of the average noise level to the inclusion brightness does not entail a significant improvement of the contrast.

Fig. 7. Graphical representation of the echo amplitudes from individual rods of the phantom, for focal points at successive distances R = 30, 50, 70, 90, 110, and 130 mm.

5. Attempt at improving the parameters of the focus

This section describes an attempt at improving the parameters of the transmitter ultrasound beam gene-

rated by the transducer sections in the ultrasonic ring array. The proposed method allowed an increase in the acoustic pressure level at a distance from the transducers to the focal point. This effect is visible to a limited extent during the excitement of $n = 32$ transducers. However, a significant improvement can be observed in the case of exciting $n = 64$ transducers. The principle of unconventional focusing is shown in Fig. 8.
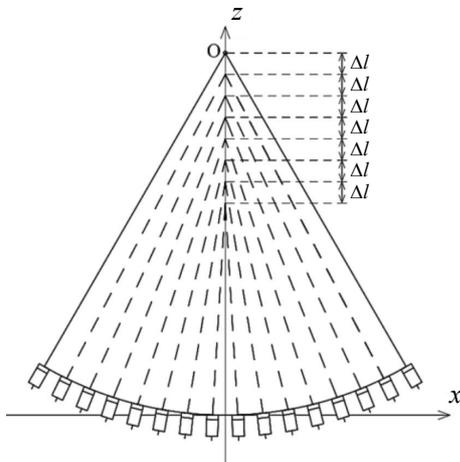
Fig. 8. Unconventional focusing method.

The principle behind the method can be described as follows. The outermost transducers are excited without any delay. The next pair of transducers towards the inside of the matrix focuses the beam directly in front of the focal point by a distance Δl closer along the symmetry axis of the ultrasonic ring array. Subsequently, the next two transducers are also focused closer by a distance Δl. Following this principle, the next pairs of transducers are re-focused until the central transducers are reached. The distance Δl is equal to the length of or to half the length of the wave propagated in the array.

The results of calculations following this method are show in Figs 9–13. The analysis included the distribution of the acoustic pressure level along a section equal to the diameter of the ring array, starting in the center of the central transducers and having the center of symmetry in the focal point resulting from the
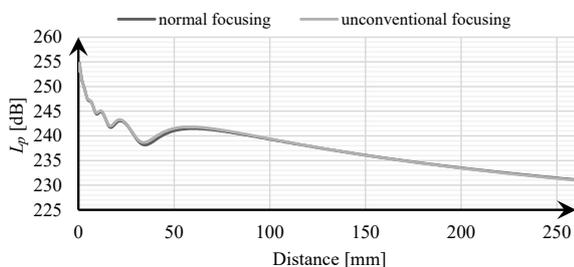
Fig. 9. Calculation results for the acoustic field distribution in the form of $L_p(x)$, $y = 0$, with the number of activated transducers $n = 32$ for normal focusing and for unconventional focusing with a shift by λ.
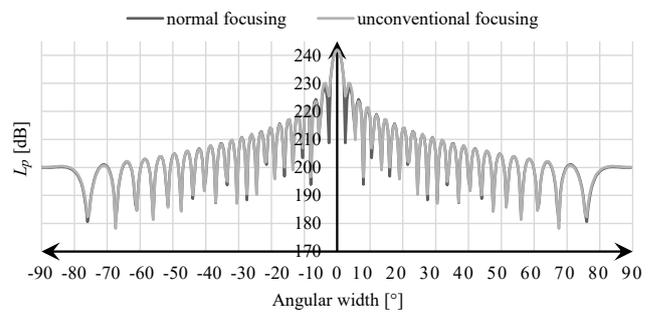
Fig. 10. Calculation results for the acoustic field distribution for the ring array in the form of $L_p(x)$ with the number of activated transducers $n = 64$ for normal focusing and for unconventional focusing with a shift by $\lambda/2$.
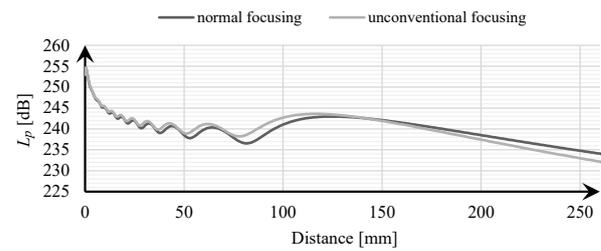
Fig. 11. Calculation results for the acoustic field distribution in the form of $L_p(x)$, $y = 0$, with the number of activated transducers $n = 64$ for normal focusing and for unconventional focusing with a shift by $\lambda/2$.
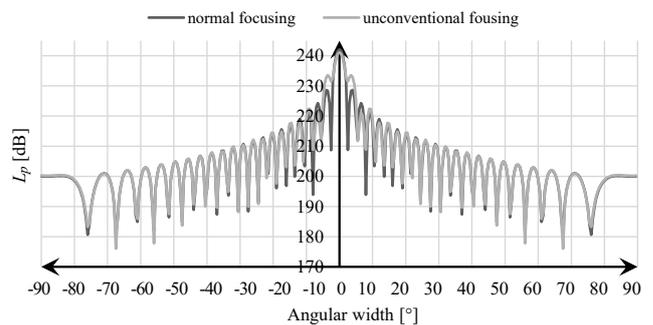
Fig. 12. Calculation results for the acoustic field distribution for the ring array in the form of $L_p(x)$ with the number of activated transducers $n = 64$ for normal focusing and for unconventional focusing with a shift by λ.
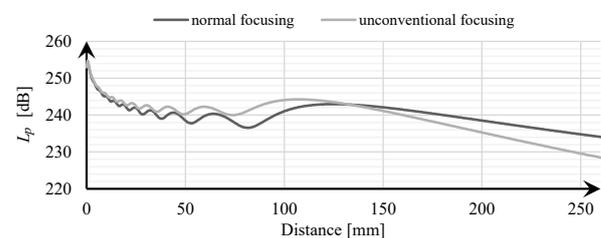
Fig. 13. Calculation results for the acoustic field distribution in the form of $L_p(x)$, $y = 0$, with the number of activated transducers $n = 64$ for normal focusing and for unconventional focusing with a shift by λ.

natural shape of the array (Figs 9, 11, and 13). The angular cross-section (Figs 10 and 12) was generated

along an arc with the curvature radius of the ring array R_p having the center of symmetry in the focal point.

The analysis of the cross-section along the main ultrasound beam demonstrates an improvement by about 0.5–1 dB in the range from 30 to 70 mm from the central transducers in the case when the focal point is shifted for successive transducers by one wavelength λ. Such a small change and a significant deviation of the focal point from the planned distance in which this focal point should occur may indicate that a single section of the ultrasonic ring array consisting of $n = 32$ transducers may be insufficient to achieve the maximum acoustic pressure level within the distance of 130 mm from the transducers.

When two matrix sections consisting of $n = 64$ ultrasonic transducers were excited as a result of unconventional focusing, accounting for the shift by $\lambda/2$ at a distance of 70–130 mm from the central transducers, i.e. directly in front of the focal point, the acoustic pressure level increased in this range by approx. 1–4 dB. In this case, the acoustic pressure level at the focal point is identical as during normal focusing. Interestingly, the width of the main lobe in the ultrasound beam has a coherence similar as in the case of normal focusing. The first side lobes are slightly elevated by about 1–2 dB.

During unconventional focusing with a shift by λ, the effect produced by improved beam parameters is even more evident. In the range from 50 to 130 mm from the central transducers, the acoustic pressure level increased by approx. 2–7 dB, and the main lobe of the ultrasound beam is as coherent as during natural focusing. The acoustic pressure level of the first side lobes also increased by 4 dB. Note should be taken of the fact that during unconventional focusing, the acoustic pressure level outside of the focal point decreases linearly faster than in the case of normal focusing.

6. Conclusions

In the proposed focusing method, the ultrasound beam will have a higher acoustic pressure level at the distance from the transducers to the focal point, and this fact will increase the amplitude of the echoes from the border of structures having different acoustic impedances. Beyond a focus distance of 130 mm, the pressure level drops, which will reduce the noise level behind the focal point. In the case when all sections of the array are successively excited, it is a favourable effect resulting from the shape of the ring array.

Due to the higher level of acoustic pressure in front of the focal point, the echoes in the range in which the beam is converging (assumes a triangular shape) will have a higher amplitude, while a lower level of acoustic pressure behind the focal point will reduce the level of noise and interference in the range where

the beam assumes a divergent shape (inverted triangle). The implementation of this procedure in the CI method should improve the contrast of an ultrasound female breast image.

The analysis of the results of the rod phantom measurements performed with the use of the ultrasonic ring array demonstrated that the ratio of the background to the echo decreases with the increase of the focusing distance from the central transducers. The greatest contrast of the image was observed in the case of focusing at a distance of 50 mm from the central transducers, when the phantom was positioned in the center of the ring array. Nevertheless, the background to echo ratio was the most favourable for focusing at a distance of 130 mm, because the tested phantom was positioned centrally in the ring array, i.e. in the focal point. During the measurements, the distance of the focal point from the examined object was observed to be the most important parameter determining the quality of the echo in the image. In the case of the female breast, which is an irregular structure, the possibility to change the focusing parameters in order for the ultrasound beam to be propagated directly in the location of the lesion should improve the quality of the ultrasound image and enable more accurate identification of the tumor.

References

1. Birk M., Kretzek E., Figuli P., Weber M., Becker J., Ruiter N.V. (2016), High-speed medical imaging in 3D ultrasound computer tomography, *IEEE Transactions on Parallel and Distributed Systems*, **27**(2): 455–467, doi: 10.1109/TPDS.2015.2405508.

2. Costaridou L. (2005), *Medical Image Analysis Method*, CRC Press Taylor & Fracis, New York.

3. Duric N. *et al.* (2007), Detection of breast cancer with ultrasound tomography: First results with the Computed Ultrasound Risk Evaluation (CURE) prototype, *Medical Physics*, **34**(2) 773–785, doi: 10.1118/1.2432161.

4. Duric N. *et al.* (2013), Breast imaging with the Soft-Vue imaging system: first results, [in:] *Medical Imaging 2013: Ultrasonic Imaging, Tomography, and Therapy. Proceedings of SPIE.SPIE*, Bosch J.G., Doyley M.M. [Eds], Vol. 8675, pp. 164–171, doi: 10.1117/12.2002513.

5. Entrekin R., Jackson P., Jago J.R., Porter B.A. (1999), Real time spatial compound imaging in breast ultrasound: Technology and early clinical experience, *Medicamundi*, **43**(3): 35–43.

6. Gudra T., Opieliński K. (2006), The ultrasonic probe for investigating of internal object structure by ultrasound transmission tomography, *Ultrasonics*, **44**(Suppl. 1): e679–e683, doi: 10.1016/j.ultras.2006.05.126.

7. Gudra T., Opieliński K. (2016), The multi-element probes for ultrasound transmission tomography, *Jour-*

nal de Physique IV, **137**: 79–86, doi: 10.1051/jp4: 2006137015.

8. GUDRA T., OPIELIŃSKI K.J. (2009), *A method of visualizing the internal structure of the center and a device for implementing this method* [in Polish: Sposób wizualizacji struktury wewnętrznej ośrodka i urządzenie do realizacji tego sposobu], Patent No 210202, Poland.

9. JIRIK R. *et al.* (2012), Sound-speed image reconstruction insparse-aperture 3-D ultrasound transmission tomography, *IEEE Transactions on Ultrasonics, Ferroelectrics, and Frequency Control*, **59**(2): 254–264, doi: 10.1109/TUFFC.2012.2185.

10. KAK A.C., SLANEY M. (2001), *Principles Computerized Tomographic Imaging*, IEEE Press, New York.

11. MARMARELIS V., JEONG J., SHIN D., DO S. (2007), High-resolution 3-D imaging and tissue differentiation with transmission tomography, [in:] *Acoustical Imaging*, André M.P. *et al.* [Eds], Vol. 28, 195–206, Springer, Dordrecht, doi: 10.1007/1-4020-5721-0_21.

12. Narodowy Instytut Onkologii im. Marii Skłodowskiej-Curie (n.d.), National Cancer Registry [in Polish: Krajowy Rejestr Nowotworów], available at https://www.pib-nio.pl/krajowy-rejestr-nowotworow/.

13. OPIELIŃSKI K.J. (2011), *Application of Transmission of Ultrasonic Waves for Characterization and Imaging of Biological Media Structures* [in Polish], Printing House of Wroclaw University of Science and Technology, Wroclaw.

14. OPIELIŃSKI K.J. *et al.* (2015), Imaging results of multi-modalultrasound computerized tomography system designed for breast diagnosis, *Computerized Medical Imaging and Graphics*, **46**(2): 83–94, doi: 10.1016/j.compmedimag.2017.06.009.

15. OPIELIŃSKI K.J. *et al.* (2016), Breast ultrasound tomography: preliminary in vivo results, [in:] *Information Technologies in Medicine*, Piętka E., Badura P.,

Kawa J., Wieclawek W. [Eds], Vol. 1, pp. 193–2015, Springer International Publishing, doi: 10.1007/978-3-319-39796-2_16.

16. OPIELIŃSKI K.J. *et al.* (2018), Multimodal ultrasound computer-assisted tomography: An approach to the recognition of breast lesion, *Computerized Medical Imaging and Graphics*, 65: 102–114, doi: 10.1016/j.compmedimag.2017.06.009.

17. OPIELIŃSKI K.J., PRUCHNICKI P., GUDRA T., MAJEWSKI J. (2014), Full angle ultrasound spatial compound imaging, [In:] *Proceedings of 7th Forum Acusticum 2014 Joined with 61st Open Seminar on Acoustics and Polish Acoustical Society – Acoustical Society of Japan Special Session Stream* [CD-ROM], Krakow: European Acoustics Association.

18. PRATAP R. (2013), *MATLAB for scientists and engineers* [in Polish: *MATLAB dla naukowców i inżynierów*], Warszawa: WN PWN.

19. STASZEWSKI W., GUDRA T. (2019), The effect of dynamic focusing of the beam on the acoustic field distribution inside the ultrasonic ring array, *Vibrations in Physical Systems*, **30**(1): 2019106, 8 pages.

20. STASZEWSKI W., GUDRA T., OPIELIŃSKI K.J. (2018), The acoustic field distribution inside the ultrasonic ring array, *Archives of Acoustic*, **43**(3): 455–463, doi: 10.24425/123917.

21. STASZEWSKI W., GUDRA T., OPIELIŃSKI K.J. (2019), The Effect of dynamic beam deflection and Focus shift on the acoustics field distribution inside the ultrasonic ring array, *Archives of Acoustics*, **44**(4): 625–636, doi: 10.24425/aoa.2019.129721.

22. WISKIN J. *et al.* (2013), Three-dimensional nonlinear inverse scattering: quantitative transmission algorithms, refraction corrected reflection, scanner design and clinical results, *Proceedings of Meetings on Acoustics*, **19**(1): 075001, doi: 10.1121/1.4800267.